HHS Public Access

Author manuscript

J Thromb Haemost. Author manuscript; available in PMC 2023 March 01.

Published in final edited form as:

J Thromb Haemost. 2022 March ; 20(3): 742–754. doi:10.1111/jth.15622.

The plasminogen receptor Plg-R_{KT} regulates adipose function and metabolic homeostasis

Fahumiya Samad[1,*], **Hongdong Bai**[2], **Nagyung Baik**[3], **Patrick Haider**[4], **Yuqing Zhang**[3], **Gersina Rega-Kaun**[4,5], **Christoph Kaun**[4], **Manfred Prager**[6], **Johann Wojta**[4,7], **Quyen Bui**[1], **Sagarika Chakrabarty**[1], **Jing Wang**[1], **Robert J. Parmer**[2,8,*], **Lindsey A. Miles**[3,*]

[1]Department of Cell Biology, San Diego Biomedical Research Institute, San Diego, CA, USA.

[2]Department of Medicine, Veterans Administration San Diego Healthcare System, San Diego.

[3]Department of Molecular Medicine, The Scripps Research Institute, La Jolla, CA.

[4]Department of Internal Medicine II, Medical University of Vienna, Vienna, Austria

[5]5th Department of Internal Medicine for Diabetes and Rheumatology, Wilhelminen Hospital, Vienna, Austria

[6]Department of Surgery, Hospital Oberwart, Oberwart, Austria

[7]Ludwig Boltzmann Institute for Cardiovascular Research, Vienna.

[8]Department of Medicine, University of California San Diego, La Jolla, CA,

Abstract

Background—Plg-R_{KT}, a unique transmembrane plasminogen receptor, enhances the activation of plasminogen to plasmin, and localizes the proteolytic activity of plasmin on the cell surface.

Objectives—We investigated the role of Plg-R_{KT} in adipose function, metabolic homeostasis and obesity.

Methods—We used adipose tissue (AT) sections from bariatric surgery patients and from high fat diet (HFD)-induced obese mice together with immunofluorescence and real-time PCR to study adipose expression of Plg-R_{KT}. Mice genetically deficient in Plg-R_{KT} and littermate controls fed a HFD or control low fat diet (LFD) were used to determine the role of Plg-R_{KT} in insulin resistance, glucose tolerance, T2D, and associated mechanisms including adipose inflammation, fibrosis, and ectopic lipid storage. The role of Plg-R_{KT} in adipogenesis was determined using 3T3-L1 preadipocytes and primary cultures established from Plg-R_{KT} deficient and littermate control mice.

Correspondence to Fahumiya Samad, 3525 John Hopkins Court, Suite, 200. San Diego, CA. 92121, USA, fsamad@sdbri.org. Lindsey Miles, 10550 N. Torrey Pines Road, SP30-3120, La Jolla, CA 92037. lmiles@scrippd.edu.

*R.J.P., L.A.M. and F.S contributed equally

Author contributions. H.B, N.B., Q. B., S.C, P.H, Y.Z, and J. Wang performed experiments and analyzed data. G. R-K., C.K., and M.P. provided human tissue samples. J. W. designed experiments and analyzed data. F.S. R.J.P., and L.A.M. designed experiments, analyzed data and wrote the manuscript.

Conflict of Interest. The authors have declared that no conflict of interest exists.

Results—Plg-R_{KT} was highly expressed in both human and mouse adipose tissue AT, and its levels dramatically increased during adipogenesis. Plg-R_{KT} deficient mice, when fed a HFD, gained more weight, developed more hepatic steatosis and were more insulin resistant/glucose intolerant than HFD-fed wild type littermates. Mechanistically, these metabolic defects were linked with increased AT inflammation, AT macrophage and T cell accumulation, adipose and hepatic fibrosis, and decreased insulin signaling in the AT and liver. Moreover, Plg-R_{KT} regulated the expression of PPARγ and other adipogenic molecules, suggesting a novel role for Plg-R_{KT} in the adipogenic program.

Conclusions—Plg-R_{KT} coordinately regulates multiple aspects of adipose function that are important to maintain efficient metabolic homeostasis.

Keywords

Plg-R_{KT}; adipose inflammation; obesity; insulin resistance; hepatic steatosis

Introduction

Metabolic, endocrine and immune functions of adipose tissue (AT) play essential roles in maintaining systemic metabolic homeostasis (1). Obesity leads to a dysfunctional AT(1), in part, due to fibrosis (2) and inflammation caused by infiltrating AT macrophages (ATM) and other immune cells (1, 3). These changes impair adipocyte insulin action and reduce AT lipid storage, leading to ectopic lipid deposition/metabolic dysfunction at non-AT sites, predominantly, liver, skeletal muscle and pancreas, and to systemic insulin resistance (IR) and glucose intolerance culminating in type 2 diabetes (T2D) (4, 5).

The plasminogen activation (PA) regulates the activity of the broad-spectrum serine protease, plasmin (6). PA to plasmin is carried out by plasminogen activators, tissue-type plasminogen activator (t-PA) and urokinase-type plasminogen activator (u-PA), while plasminogen activator inhbitor-1 (PAI-1) is the primary physiological inhibitor of PA *in vivo*.(7) While plasmin is the major enzyme responsible for degradation of fibrin (8, 9), it also regulates extracellular matrix (ECM) remodeling, fibrosis and inflammation (reviewed in (10, 11)), processes that profoundly affect adipose function and systemic metabolism (2). A key role for inhibitors of PA and for pro-thrombotic pathways in promoting the sequelae of obesity is well established (12–14). PAI-1 and Tissue Factor (TF) are increased in AT of obese mice (12, 13, 15–18) and humans (14, 18–20) and are linked to IR/T2D (12) (13, 14) consistent with a major role for adipose fibrosis and excessive fibrin deposition in this process (2). More recent studies have shown that thrombin-dependent fibrin formation drives inflammation, weight gain, glucose dysmetabolism and steatosis in diet induced obesity (21). However, studies addressing the role of the pro-fibrinolytic arm of the fibrinolytic system in AT pathogenesis are limited. Mice deficient in t-PA develop exacerbated obesity on a high fat diet (HFD) (22). Mice deficient in plasminogen exhibit impaired adipocyte differentiation when fed a HFD and, also, during mammary gland involution(23, 24).

Plg-R_{KT}, is a structurally unique transmembrane plasminogen receptor, which enhances the activation of plasminogen to plasmin, and localizes the proteolytic activity of plasmin on the cell surface (25)' In genome wide association studies the PLGRKT (C9orf46) gene

was identified as a novel genetic locus for the pathophysiology of childhood obesity(26), and has also been found to be associated with polycystic ovarian syndrome, which in turn is associated with obesity, insulin resistance, and T2D (50,51). Plasmin-dependent mononuclear cell migration to inflammatory sites is regulated by Plg-R_{KT} (27–30). In addition, plasmin-dependent cytokine release from macrophages is promoted by Plg-R_{KT} (29, 30). Interestingly, Plg-R_{KT} $^{-/-}$ females are unable to lactate, consistent with inability to remodel ECM during epithelial migration and impaired adipose remodeling during lactational development (31). Here, we uncovered a novel role of Plg-R_{KT}, in adipose function and systemic metabolism. Our results demonstrate that Plg-R_{KT} is a crucial regulator of weight gain and adipogenesis as well as other major sequelae of obesity including adipose inflammation, hepatic steatosis and insulin resistance, and that Plg-R_{KT} plays a key role in promoting healthy adipose function and maintaining systemic metabolic homeostasis.

Research Design and Methods

Mice.

Studies were approved by Institutional Animal Care and Use Committees (The Scripps Research Institute and University of California, San Diego). Plg-R_{KT} gene targeted mice (31) were backcrossed ten generations into the C57Bl/6J background. Beginning at 8–10 weeks of age, male Plg-$R_{KT}^{-/-}$ mice and Plg-$R_{KT}^{+/+}$ littermates were placed on a HFD (D12492, 60% kcals from fat, Research Diets, New Brunswick NJ) or control low fat diet (LFD,D12450J, 10 kcal % fat, matching sucrose to D12492, Research Diets). Body weights were obtained weekly.

Human subjects

Studies were approved by the University of Vienna ethics committee and performed according to the declaration of Helsinki (29). AT was obtained from morbidly obese patients undergoing gastric bypass surgery.

Metabolic parameters.

Glucose tolerance tests (GTT) were performed on mice fasted for 6 h and insulin tolerance tests (ITT) on non-fasted mice (16). Mice were injected i.p. with glucose (2 g/kg BW) or human insulin (0.75 U/kg, Humulin; Eli Lilly, Indianapolis, IN) and blood drawn via the tail vein at baseline and indicated intervals post-injection. Plasma insulin levels were measured with an insulin assay kit (Mercodia Ultrasensitive Insulin ELISA; Alpco Diagnostics, Salem NH), glucose was monitored with the Easy Step Blood Glucose Diabetic Monitor Meter System Model #91237. Total fat and lean mass were obtained via EchoMRI.

Fibrinogen:

Levels were determined using an ELISA kit from Innovative Research Inc. Novi, MI according to the manufacturer’s instructions.

Insulin signaling and western blot analysis.

For insulin signaling experiments, mice were injected through the tail vein with 0.75 U/kg of human insulin or saline and sacrificed 10 min later. Liver, epididymal adipose tissue (EAT), and muscle were collected, for western blot analysis with antibodies to Akt, phospho-Akt, and β-actin (Cell Signaling Technology). For UCP-1, UCP-2 and fibrin analysis relevant tissues were collected for western blot analysis with antibodies to UCP-1 (Abcam, Waltham, MA), UCP2 (Proteintech, Rosemont, IL) and fibrinogen (Dako, Santa Clara, CA). Tissues were lysed in RIPA buffer (Sigma) with protease and phosphatase inhibitors (Thermo Fisher Scientific), electrophoresed and transferred to nitrocellulose membranes. Membranes were incubated with primary antibodies, washed with PBS-containing-0.1% Tween-20 and incubated with species specific IRDye®680RD/800CW-conjugated secondary antibodies. Immunoreactive bands were visualized using the Odyssey Imaging System (LI-COR) and densitometric quantification performed using Image Studio™ Lite Software 5.2 (LI-COR).

Adipose tissue fractionation, primary adipocyte cultures and Oil Red O staining:

AT was minced in PBS containing 0.5% BSA and incubated at 37°C with collagenase (1 mg/ml in PBS/0.5% BSA) for 20 min on a shaking platform. The mixture was filtered through a 250 μm filter, centrifuged (5 min, at 200g at 4°C), and the pellet recovered as the SVF (16, 32). The SVF was incubated in RBC lysis buffer (5 min), resuspended and cultured in DMEM containing 10% FBS. The media was changed 2 hours after plating and adipogenesis induced when preadipocyte cultures were 100% confluent by treating cells with 200 nM insulin, 250 nM dexamethasone and 0.5 mM isobutyl methylxanthine (Sigma-Aldrich) for 3 days and then in the absence of differentiating agents, with media replaced every 2 days. Ten days post-differentiation, cells were stained with Oil Red O and also harvested for mRNA isolation and gene analysis. For Oil Red O staining, cells were fixed with 10% PBS buffered formalin for at least 12 hr at 4°C. Cells were stained for one hour with Oil Red O solution (5 g/L in isopropyl alcohol) and washed with distilled water

Flow cytometry.

Flow cytometry of EAT-derived SVF cells was performed as previously described (16, 32). Briefly, cells in FACS buffer (PBS containing 1% fetal calf serum and 1 mM EDTA) were stained at 4°C for 30 min with fluorophore-labeled monoclonal antibodies to F4/80, CD11c, CD3, CD4 and CD8 (eBioscience) in the presence of Fc receptor blocking antibodies (anti-CD16/CD32; eBioscience). Cells were washed, fixed in 1% formaldehyde, and analyzed on an LSR-II cytometer (BD Biosciences) with data processing using FlowJo (Tree Star).

Real-time quantitative RT-PCR.

cDNAs synthesized from total RNA (Ultraspec RNA isolation system; Biotecx Laboratories) were analyzed with gene-specific primer sets (Invitrogen) and SYBR Green PCR Master mix (PerkinElmer) in an iCycler (Bio-Rad) (16, 32). Relative gene expression levels were calculated after normalization to β-actin using the ΔΔCT method (Bio-Rad).

Real-time quantitative RT-PCR primer sets used are as follows.

$PlgR_{KT}$	Left primer	5’ ggc att gca acc atc tct tt 3’
	Right primer	5’ gtt ccg tag ccc agg tca ta 3’
B-actin	Left primer	5’ tgg aat cct gtg gca tcc atg aaa c
	Right primer	5’ taa aac gca gct cag taa cag tcc g
GAPDH	Left primer	5’ cca gta tga ctc cac tca cg 3’
	Right primer	5’ gac tcc acg aca tac tca gc 3’
TNFα	Left primer	5 cgt cag ccg att tgc tat ct 3
	Right primer	5 cgg act ccg caa agt cta ag 3
IL6	Left primer	5 gac aac cac ggc ctt ccc ta 3
	Right primer	5 gcc tcc gac ttg tga agt ggt 3
CCL2	Right primer	5 agc acc agc caa ctc tca c 3
	Left primer	5 tct gga ccc att cct tct tg 3
IFNγ	Left primer	5 tca agt ggc ata gat gtg gaa gaa 3
	Right primer	5 tgg ctc tgc agg att ttc atg 3
IL-1β	Left primer	5 tgg gat cct ctc cag cca ag 3
	Right primer	5 tgc cac agc ttc tcc aca gc 3
PPARγ	Left primer	5 ctg tcg gtt tca gaa gtg cct 3
	Right primer	5 ccc aaa cct gat ggc att gtg aga ca 3
Adiponectin	Left primer	5 ctc ctg ctt tgg tcc ctc ca 3
	Right primer	5 gtg cca tct ctg cca tca cg 3
AP2	Left primer	5 ctg gac ttc aga ggc tca tag ca 3
	Right primer	5 tac tct ctg acc gga tgg tga cca a 3
LPL	Left primer	5 ttc tcc tcc tac tcc tcc tc 3
	Right primer	5 tgt cct cag ctg tgt ctt ca 3
F4/80	Left primer	5 tgg ctg cct ccc tga ctt tc 3
	Right primer	5 caa gat ccc tgc cct gca ct 3

Digital droplet PCR (ddPCR).

All ddPCR measurements were made using the QX200 Droplet Digital PCR System from Bio-Rad following manufacturer’s recommended protocol. We followed the iScript Advanced cDNA synthesis protocol to convert RNA to cDNA and used the ddPCR Evagreen protocol for target detection. ddPCR was performed using the EvaGreen ddPCR kit with PCR primers diluted to a final concentration of 250 nM in the PCR mix.

Histology, trichrome staining, immunohistology, immunofluorescence.

Formalin-fixed, paraffin-embedded sections of adipose and liver were stained with either H & E or mason’s trichrome stain. For fibrin immunohistology, AT sections were incubated overnight at 4ºC with the primary antibody, polyclonal rabbit anti-human fibrinogen (A0080 from Dako), The slides were washed and treated sequentially with biotinylated goat anti-rat IgG (Jackson Immunoresearch), streptavidin-peroxidase conjugate (Zymed), and diaminobenzidine chromogen containing 0.03% hydrogen peroxide (Vector Laboratories), counterstained with Gill modified hematoxylin, and mounted in GVA-mount (Zymed).

Immunofluorescence staining for Plg-R_{KT} in human and mouse AT was done using the pan specific primary antibody mouse anti- PlgR_{KT} mAb 7H1 previously described (38). Human adipose macrophages were stained using rabbit anti-CD80 Ab (Santa Cruz Biotechnology) and mouse ATM stained using rat anti-F4/80 Ab (ThermoFisher). Quantitative analysis of immunohistochemical data was done using QuPath v0.3.0.

Hepatic triglyceride:

Hepatic triglyceride was measured as previously described (16). Briefly, liver samples (20–30mg) were homogenized in isopropanol, centrifuged (2000g, 10min) and 100 μl of supernatant dried in a Speedvac, dissolved in isopropanol and assayed for triglyceride content with a Triglyceride E test (Wako).

Statistical analysis.

The statistical significance of differences between groups was analyzed using repeated measures ANOVA and unpaired Student's t-test.

Data and Resource Availability.

Data and resources from this article are available from the corresponding authors upon request.

Results

Plg-R_{KT} is expressed in human and murine adipose tissues

We performed immunofluorescence studies for Plg-R_{KT} expression on AT sections from obese human bariatric patients. Distinct staining for Plg-R_{KT} was observed around the periphery of adipocyte cell membranes of omental visceral adipose tissue (OVAT) (Fig.1 A–a), abdominal subcutaneous adipose tissue (ASAT) (Fig.1 A–b) and mesenteric visceral adipose tissue (MVAT) (Fig.1 A–c). Plg-R_{KT} expression in ATM in each of the human adipose depots was observed and was identified by co-staining of Plg-R_{KT} and the macrophage marker CD80 (Fig. 1B). These adipose macrophages staining for Plg-R_{KT} appear to be in crown-like structures surrounding adipocytes (Fig. 1B–d, B–h, B–i).

Plg-R_{KT} expression in adipocytes was also observed in epididymal AT from HFD-fed obese mice (Fig. 2–a). In murine AT, Plg-R_{KT} expression was also expressed in ATM as seen in co-localization of Plg-R_{KT} with cells that stained with the mouse macrophage marker F4/80 and accumulated in crown-like structures (Fig. 2b–2e). Controls show that Plg-R_{KT} expression was not observed in Plg-$R_{KT}^{-/-}$ mice (Fig. 2f) while these mice stained for the macrophage marker F4/80 (Fig. 2g).

We next determined PlgR_{KT} gene expression in male C57BL/6J mice that were fed either a HFD or a LFD of normal chow for 16 weeks. Compared with mice fed the LFD, mice on the HFD had significantly lower expression of Plg-R_{KT} mRNA in epididymal AT (Fig. 3A) and in adipocytes isolated from EAT (Fig. 3B, C). In ATM, Plg-R_{KT} gene expression, although not statistically significant, was modestly increased (Fig. 3C).

Deletion of Plg-R_{KT} results in exaggerated weight gain and altered body fat distribution in response to high fat feeding

To address the role of Plg-R_{KT} in obesity and metabolism, we compared the metabolic consequences of a HFD in mice genetically deficient in Plg-R_{KT} (Plg-$R_{KT}^{-/-}$) and Plg-$R_{KT}^{+/+}$ littermates. Mice were weighed weekly from weeks 0–14 and again at week 16 at sacrifice. Over the course of the feeding regime, HFD-fed Plg-$R_{KT}^{-/-}$ and Plg-$R_{KT}^{+/+}$ gained significantly more weight compared to mice fed the LFD (Fig. 3D). Beginning as early as 4 weeks, HFD-fed Plg-$R_{KT}^{-/-}$ mice gained significantly more weight than HFD-fed Plg-$R_{KT}^{+/+}$ littermates (Fig. 3D) whereas no genotype-dependent differences in weight were observed between LFD-fed Plg-$R_{KT}^{-/-}$ and Plg-$R_{KT}^{+/+}$ littermates (Fig. 3D). HFD-fed Plg-$R_{KT}^{-/-}$ mice continued to gain weight resulting in a greater difference in body weight ($P<0.001$) compared to HFD-fed Plg-$R_{KT}^{+/+}$ mice at 16 weeks post initiation of HFD feeding (Fig. 3E).

Body composition studies as measured by EchoMRI after 16 weeks on the HFD revealed that Plg-$R_{KT}^{-/-}$ mice had significantly higher total fat mass (including all fat in adipose + non-adipose organs) compared to Plg-$R_{KT}^{+/+}$ littermates (Fig. 3F). In contrast, EAT weight was significantly lower in HFD-fed Plg-$R_{KT}^{-/-}$ mice when compared to Plg-$R_{KT}^{+/+}$ littermates (Fig. 3G,H). In parallel with the decrease in EAT weight, liver weights were significantly increased in HFD-fed Plg-$R_{KT}^{-/-}$ mice compared to HFD-fed Plg-$R_{KT}^{+/+}$ littermates (Fig. 3I, J). The weights of the inguinal subcutaneous adipose (SAD), heart, and kidney of HFD-fed Plg-$R_{KT}^{-/-}$ mice showed modest increases compared to Plg-$R_{KT}^{+/+}$ littermates that were not statistically significant (Fig. 3K, L, M). EchoMRI data also showed a significant increase in lean mass in HFD-fed Plg-$R_{KT}^{-/-}$ mice (Fig. 3N).

Histological analysis indicated that steatosis was increased in 16-week HFD-fed Plg-$R_{KT}^{+/+}$ mice compared with Plg-$R_{KT}^{+/+}$ mice fed a LFD of normal chow (Fig. 4A–a, Fig. 4A–b). Steatosis was further dramatically exacerbated in HFD-fed Plg-$R_{KT}^{-/-}$ mice compared with HFD-fed Plg-$R_{KT}^{+/+}$ littermates (Fig. 4A–b, Fig.4A–c). In parallel, triglyceride accumulation was significantly higher in the livers of HFD-fed Plg-$R_{KT}^{-/-}$ mice compared with Plg-$R_{KT}^{+/}$ littermates (Fig. 4B). Moreover, the exacerbated steatosis in HFD-fed Plg-$R_{KT}^{-/-}$ mice was accompanied by significant hepatocellular damage as shown by an increase in serum alanine aminotransferase, an enzymatic biomarker of hepatocyte membrane damage (Fig. 4C).

Lipid accumulation was also observed in other insulin sensitive organs that contribute to systemic glucose homeostasis. Brown fat of both LFD and HFD-fed Plg-$R_{KT}^{+/+}$ mice displayed a typical brown fat morphology with cells accumulating multiple small lipid droplets (Fig. 5A). In contrast, in the brown fat depots of HFD-fed Plg-$R_{KT}^{-/-}$ mice a predominant number of cells took on a white fat morphology with large unilocular lipid droplets (Fig.5A). In parallel with the change to a “white fat” morphology, both UCP-1 (Fig. 5B, 5C) and UCP-2 (Fig. 5D) expression levels were decreased in HFD-fed Plg-$R_{KT}^{-/-}$ mice. Increased fat deposition was also observed in skeletal muscle (Fig.5E) and modestly increased in the pancreas (Fig.5F) of HFD-fed Plg-$R_{KT}^{-/-}$ compared with HFD-fed Plg-$R_{KT}^{+/+}$ littermates. In addition to increased lipid accumulation, accumulation

of inflammatory cells were observed in the vicinity of islets in HFD-fed Plg-$R_{KT}^{-/-}$ mice (Fig.5F).

Deletion of Plg-R_{KT} results in increased adipose inflammation and immune cell accumulation

To determine the cellular and molecular mechanisms of blunted EAT expansion and increased ectopic lipid deposition in HFD-fed Plg-$R_{KT}^{-/-}$ mice, we performed histological and molecular analysis of EAT. H & E staining showed dramatically increased inflammatory cell infiltrates in EAT of HFD-fed Plg-$R_{KT}^{-/-}$ (Fig. 4E). Gene expression analysis identified multiple transcriptional changes in AT of HFD-fed Plg-$R_{KT}^{-/-}$ mice that were consistent with an inflammatory phenotype. Notably, TNF-α, IL-6, CCL2, IFNγ and IL-1β levels in AT were higher in HFD-fed Plg-$R_{KT}^{-/-}$ mice (Fig. 4F).

By FACS analysis we found that a population of macrophages with the surface marker signature F4/80+/CD11c+ (M1-like macrophages) and a population expressing F4/80+/CD11c- (M2-like macrophages) were significantly increased in epididymal AT of HFD-fed Plg-$R_{KT}^{-/-}$ mice compared to HFD-fed Plg-$R_{KT}^{+/+}$ littermates (Fig.4G,H). A markedly higher number of CD8+T effector cells was observed in the epididymal AT of Plg-$R_{KT}^{-/-}$ mice compared with Plg-$R_{KT}^{+/+}$ littermates whereas the number of CD4+T cells was less in Plg-$R_{KT}^{-/-}$ mice (Fig. 4I, J). In the liver, exacerbated steatosis of HFD-fed Plg-$R_{KT}^{-/-}$ mice was also accompanied by higher levels of inflammatory cytokines including TNFα, IL-6, IL-1β and CCL2, as well as the macrophage marker F4/80 (Fig. 4D).

Deletion of Plg-R_{KT} results in increased adipose and liver fibrosis

To determine whether Plg-R_{KT} regulates fibrosis we performed Masson's trichrome staining and immunohistochemistry for fibrin deposition on EAT and liver tissue sections from HFD-fed Plg-$R_{KT}^{-/-}$ mice and HFD-fed Plg-$R_{KT}^{+/+}$ littermates. Trichrome staining of EAT revealed modest collagen (blue) staining in epididymal AT of HFD- Plg-$R_{KT}^{+/+}$ mice (Fig. 6A). In comparison, HFD-fed Plg-$R_{KT}^{-/-}$ tissue showed markedly greater collagen deposition (Fig. 6B). Immunohistochemical analysis showed higher levels of fibrin in EAT of HFD-fed Plg-$R_{KT}^{-/-}$ (Fig. 6D, E) compared with Plg-$R_{KT}^{+/+}$ mice (Fig. 6C). Quantification of fibrin using QuPath software confirmed a significant increase in fibrin in EAT of HFD-fed Plg-$R_{KT}^{-/-}$ (Fig. 6I). Compared to HFD- Plg-$R_{KT}^{+/+}$ mice (Fig. 6F) immunohistochemical staining also revealed excessive fibrin in the livers of HFD-fed Plg-$R_{KT}^{-/-}$ mice (Fig. 6G, H), and this was also confirmed by quantification of fibrin by QuPath analysis (Fig. 6J). In parallel with the increased fibrin deposition in adipose and liver, we found that plasma fibrinogen levels were elevated in HFD-fed Plg-$R_{KT}^{-/-}$ mice compared to HFD-fed Plg-$R_{KT}^{+/+}$ littermates (Fig. 6K).

HFD-fed Plg-$R_{KT}^{-/-}$ mice exhibit increased glucose intolerance and insulin resistance

We tested whether adipose inflammation/fibrosis and ectopic lipid accumulation in HFD-Plg-$R_{KT}^{-/-}$ mice mechanistically translated into an exacerbation of blunted glucose homeostasis. Fasting plasma insulin and glucose levels were significantly higher in HFD-fed Plg-$R_{KT}^{-/-}$ mice compared with HFD-fed Plg-$R_{KT}^{+/+}$ littermates, (Fig. 7A,B). In glucose tolerance tests (GTT), HFD-fed Plg-$R_{KT}^{-/-}$ mice were less efficient in clearing an

intraperitoneal injection of glucose (Fig. 7C). HFD-fed Plg-$R_{KT}^{-/-}$ mice also demonstrated decreased insulin sensitivity, shown by less efficient insulin-mediated suppression of plasma glucose in insulin tolerance tests (ITT) (Fig. 7D). No genotype-dependent differences were observed for either GTT or ITT when mice were fed a normal chow diet (data not shown).

To obtain mechanistic insights into the tissue-specific contribution of Plg-R_{KT} to insulin signaling we assessed the extent to which changes in the insulin signaling pathways in adipose, liver and muscle contributed to the decreased systemic insulin sensitivity of HFD-fed Plg-$R_{KT}^{-/-}$ mice. In response to an insulin injection, the phosphorylation of Akt, a primary insulin signaling molecule, was severely blunted in the EAT and liver of HFD-fed Plg-$R_{KT}^{-/-}$ mice compared with Plg-$R_{KT}^{+/+}$ littermates (Fig. 7E, F). In contrast, in muscle Akt phosphorylation was similar in HFD-fed Plg-$R_{KT}^{-/-}$ and Plg-$R_{KT}^{+/+}$ littermates (Fig. 7G).

Plg-R_{KT} regulates adipogenic pathways

Decreased EAT weight (Fig.3G, H) together with increased ectopic lipid accumulation (Fig. 4A, Fig. 5) in HFD-fed Plg-$R_{KT}^{-/-}$ mice may indicate that the loss of Plg-R_{KT} impairs adipogenesis. Indeed, we found that the gene expression of the key adipogenic transcription factor, PPARγ, was lower in the EAT of HFD-fed Plg-$R_{KT}^{-/-}$ mice compared with that of HFD-fed Plg-$R_{KT}^{+/-+}$littermates (Fig. 8A). To further study the potential role of Plg-R_{KT} in adipogenesis we determined how its expression was regulated during the differentiation of 3T3-L1 pre-adipocytes to adipocytes. Plg-R_{KT} mRNA and protein expression were low in pre-adipocytes, but dramatically increased during adipogenesis (Fig. 8 B,C,D); a pattern of expression similar to that of other mediators/signaling pathways that are required for adipogenesis (33). Concordant with increased Plg-R_{KT} expression, plasminogen binding was also increased in adipocytes compared to pre-adipocytes (Fig. 8E). We determined whether blocking plasminogen binding to its receptor, Plg-$R_{KT,}$ might interfere with the adipogenic gene expression program. Treatment of 3T3-L1 pre-adipocytes with anti-Plg-R_{KT} mAB(7H1) (34) during adipogenesis resulted in decreased expression of PPARϒ, as well as PPARγ adipogenic target genes including adiponectin, AP2 and LPL (Fig. 8F). To confirm the relationship between adipogenesis and Plg-R_{KT} we compared adipogenesis of stromal vascular fraction (SVF) cells from AT of Plg-$R_{KT}^{-/-}$ and Plg-$R_{KT}^{+/+}$ littermates. Plg-$R_{KT}^{-/-}$ SVF cells showed decreased adipogenesis as indicated by Oil Red O staining of adipocytes (Fig. 8G) and decreased expression of PPARγ and its adipogenic target, AP2, (Fig. 8H) indicating decreased adipogenic potential of pre-adipocytes that lack Plg-R_{KT}.

Discussion

These studies investigated the role of the pro-fibrinolytic plasminogen receptor, Plg-R_{KT}, in adipose function, metabolic homeostasis and obesity. We found that Plg-R_{KT} was highly expressed in both human and mouse AT. Strikingly, HFD-fed Plg-$R_{KT}^{-/-}$ mice gained more total body weight while exhibiting lower EAT weight, were more insulin resistant/glucose intolerant, and developed more hepatic steatosis than HFD-fed Plg-$R_{KT}^{+/+}$ littermates. These metabolic abnormalities were mechanistically associated with increased AT and liver inflammation, increased ATM and T cell accumulation, and increased adipose

and hepatic fibrosis, ultimately blunting insulin signaling in the AT and liver leading to increased systemic IR and glucose intolerance. Furthermore, Plg-R_{KT} regulated expression of the key adipogenic transcription factor, PPARγ, suggesting a novel role for Plg-R_{KT} in the adipogenic program. Thus, Plg-R_{KT} coordinately regulates multiple aspects of adipose function that are important to maintain efficient metabolic homeostasis.

The capacity of AT to remodel and expand is crucial for accommodating changes in energy availability and metabolic homeostasis, and blunted adipogenesis is observed in AT of obese/insulin resistant subjects. Our studies indicate that Plg-R_{KT} is a unique receptor that promotes adipogenesis. This is based on the following observations: a) The adipogenic transcription factor PPARγ was decreased in the AT of HFD-fed-Plg-$R_{KT}^{-/-}$ mice; b) Plg-R_{KT} expression and plasminogen binding increased during adipogenesis of 3T3-L1 adipocytes, an expression pattern reminiscent of mediators/signaling pathways that are required for adipogenesis (33); c) Treatment of 3T3-L1 preadipocytes with an inhibitory antibody to Plg-R_{KT} during differentiation decreased the expression of PPARγ and adipogenic genes including adiponectin, AP2 and LPL; d) Adipogenesis was dramatically blunted in primary adipocyte cultures derived from adipose SVF cells from Plg-$R_{KT}^{-/-}$ mice compared to adipocyte cultures from wild type littermates.

In the current study we found a redistribution of lipids from EAT to other tissues; decreased EAT weight paralleled increased liver weight and steatosis, lipid deposition in muscle and pancreas, and enhanced “whitening” of brown fat depots. Brown AT catabolizes glucose and fatty acids to produce heat and regulates systemic metabolism and glucose homeostasis (35). “Whitening” of brown AT characterized by increased lipid deposition and mitochondrial dysfunction contributes to systemic IR and glucose intolerance (36, 37). Enhanced “whitening” and decreased expression of thermogenic markers UCP-1 and UCP-2 observed in the brown AT of HFD-fed Plg-$R_{KT}^{-/-}$ mice in comparison to similarly fed Plg-$R_{KT}^{+/+}$ littermates suggests that Plg-R_{KT} may have a unique role in maintaining brown AT function.

In response to an intravenous injection of insulin, HFD-fed Plg-$R_{KT}^{-/-}$ mice showed a marked reduction in Akt phosphorylation in AT and liver compared to HFD-fed Plg-$R_{KT}^{+/+}$ mice. These results point to the primary involvement of Plg-R_{KT} in the adipose and liver in maintaining glucose homeostasis. The mechanism(s) by which the loss of Plg-R_{KT} blunts Akt phosphorylation may be indirectly related to increased adipose and liver inflammation and fibrosis. Additionally, a direct signaling mechanism cannot be excluded. Whereas Plg-R_{KT} has only a short 4 amino acid cytoplasmic domain (25), its signaling effects are likely to be mediated by association with other signaling molecules as in the case with uPAR, a GPI-linked receptor that regulates intracellular signaling (38).

Macrophages accumulate in AT of obese mice and humans and contribute to obesity-induced IR (1, 39, 40). Deletion of chemokine (C-C motif) ligand 2 (CCL2) reduces ATM accumulation and improves insulin sensitivity (41), and overexpression of CCL2 promotes insulin resistance (42). Notably, CCL2 expression was increased in AT of HFD-fed Plg-$R_{KT}^{-/-}$ mice. Obese AT shows high expression of both M2-like and M1-like macrophages and areas of fibrosis in obese AT contain many M2-like macrophages (43). In this respect,

it is noteworthy that Plg-R_{KT} has been shown to be expressed in both M1-like and M2-like macrophages (29). Increased inflammatory cell infiltrates were observed associated with areas of fibrosis in AT of HFD-fed Plg-$R_{KT}^{-/-}$ mice and both M1-like and M2-like ATM populations were increased in HFD-fed Plg-$R_{KT}^{-/-}$ mice. The increased cellular infiltrate is noteworthy in view of the requirement for Plg-R_{KT} for macrophage recruitment in experimental peritonitis (44). Similar cellular infiltrates are observed in spontaneously thrombotic organs of plasminogen deficient mice (9, 45), although plasminogen deficient mice also exhibit defective macrophage recruitment in experimental peritonitis (46). These differences may relate to differential expression of Plg-R_{KT} on different monocyte subsets (29). In addition to macrophage changes in AT, adipose T cell populations also regulate obesity-associated inflammation and insulin sensitivity (47). Increased CD8+ effector T cells are observed in the AT of obese rodents and humans, while some studies also report a parallel decrease in CD4+ helper T cells (47). Similarly, we observed increased levels of CD8+ T cells and diminished CD4+ T cell populations in EAT of Plg-$R_{KT}^{-/-}$ mice, compared to Plg-$R_{KT}^{+/+}$ littermates. This is the first report of a role of Plg-R_{KT} in T cell trafficking.

Procoagulant and anti-fibrinolytic pathways accelerate the development of dysfunctional AT in response to obesity (12, 13, 15–18) (14). The mechanism likely relies on excessive fibrin deposition, leading to recruitment and proliferation of macrophages in the AT with subsequent development of the sequelae of obesity (2, 48, 49). The role of pro-fibrinolytic pathways has not been extensively investigated. Consistent with a role for fibrin degradation, t-PA-deficient mice develop exacerbated obesity on a HFD (22). Plasminogen-deficient mice however exhibit a phenotype with poor health and significant weight loss during development (9,23) which makes comprehensive metabolic studies more difficult in the plasminogen null mouse model and, hence it is challenging to directly compare metabolic profiles of plasminogen deficient mice with Plg-$R_{KT}^{-/-}$ mice. Decreased fibrin degradation and inability to remodel the ECM in dysfunctional AT appeared to contribute to the exacerbated response to obesity in HFD-fed-Plg-$R_{KT}^{-/-}$ mice. However, uniquely, Plg-R_{KT} appears to be required for healthy adipogenesis, which may be a key mechanism by which Plg-R_{KT} regulates the response to obesity, and which may be distinct from thrombin and fibrin-generating procoagulant pathways and may involve the interaction of Plg-R_{KT} with heretofore unidentified ligands. Defects in adipogenesis in HFD-fed-Plg-$R_{KT}^{-/-}$ mice may result in excessive accumulation of ECM and subsequent recruitment of macrophages and pro-inflammatory cytokine release in AT that feeds back to further decrease adipogenesis. Defective adipogenesis may also result in ectopic fat deposition and steatosis in liver, muscle, pancreas, and brown fat. Thus, Plg-R_{KT} provides a novel control point for the maintenance of efficient metabolic homeostasis at multiple key regulatory steps.

Acknowledgements.

NIH Grants HL149511 (to F.S., R.J.P. and L.A.M.), HL-104232 (to F.S.), HL-081046 (to L.A.M.), Austrian National Bank Jubilaeumsfondsprojekt No. 16377 (to G.R.K.), Austrian Science Fund SFB-5412 (to J.W.), Merit Review Award I01BX003933 from the U.S. Department of Veterans Affairs (to R.J.P.) We thank Amanda J Roberts and the Scripps Research Animal Core Facility for the EchoMRI services.

References

1. Olefsky JM, and Glass CK. Macrophages, inflammation, and insulin resistance. Annu Rev Physiol. 2010;72:219–46. [PubMed: 20148674]
2. Sun K, Tordjman J, Clement K, and Scherer PE. Fibrosis and adipose tissue dysfunction. Cell Metab. 2013;18(4):470–7. [PubMed: 23954640]
3. Russo L, and Lumeng CN. Properties and functions of adipose tissue macrophages in obesity. Immunology. 2018;155(4):407–17. [PubMed: 30229891]
4. Hammarstedt A, Gogg S, Hedjazifar S, Nerstedt A, and Smith U. Impaired Adipogenesis and Dysfunctional Adipose Tissue in Human Hypertrophic Obesity. Physiol Rev. 2018;98(4):1911–41. [PubMed: 30067159]
5. Shulman GI. Ectopic fat in insulin resistance, dyslipidemia, and cardiometabolic disease. N Engl J Med. 2014;371(12):1131–41. [PubMed: 25229917]
6. Urano T, Castellino FJ, and Suzuki Y. Regulation of plasminogen activation on cell surfaces and fibrin. J Thromb Haemost. 2018.
7. Loskutoff DJ, and Schleef RR. Plasminogen activators and their inhibitors. Methods Enzymol. 1988;163:293–302. [PubMed: 3148826]
8. Bugge TH, Flick MJ, Daugherty CC, and Degen JL. Plasminogen deficiency causes severe thrombosis but is compatible with development and reproduction. Genes Dev. 1995;9(7):794–807. [PubMed: 7705657]
9. Ploplis VA, Carmeliet P, Vazirzadeh S, Van V,I, Moons L, Plow EF, et al. Effects of disruption of the plasminogen gene on thrombosis, growth, and health in mice. Circulation. 1995;92(9):2585–93. [PubMed: 7586361]
10. Deryugina EI, and Quigley JP. Cell surface remodeling by plasmin: a new function for an old enzyme. J Biomed Biotechnol. 2012;2012:564259. [PubMed: 23097597]
11. Miles LA, and Parmer RJ. Plasminogen receptors: the first quarter century. Semin Thromb Hemost. 2013;39(4):329–37. [PubMed: 23532575]
12. Samad F, and Loskutoff DJ. Tissue distribution and regulation of plasminogen activator inhibitor-1 in obese mice. Mol Med. 1996;2:568–82. [PubMed: 8898373]
13. Samad F, Uysal KT, Wiesbrock SM, Pandey M, Hotamisligil GS, and Loskutoff DJ. Tumor necrosis factor α is a key component in the obesity-linked elevation of plasminogen activator inhibitor-1. Proc Natl Acad Sci USA. 1999;96:6902–7. [PubMed: 10359811]
14. Alessi MC, and Juhan-Vague I. Metabolic syndrome, haemostasis and thrombosis. Thromb Haemost. 2008;99(6):995–1000. [PubMed: 18521499]
15. Shah C, Yang G, Lee I, Bielawski J, Hannun YA, and Samad F. Protection from high fat diet-induced increase in ceramide in mice lacking plasminogen activator inhibitor 1. J Biol Chem. 2008;283(20):13538–48. [PubMed: 18359942]
16. Badeanlou L, Furlan-Freguia C, Yang G, Ruf W, and Samad F. Tissue factor-protease-activated receptor 2 signaling promotes diet-induced obesity and adipose inflammation. Nat Med. 2011;17(11):1490–7. [PubMed: 22019885]
17. Samad F, Pandey M, and Loskutoff DJ. Tissue factor gene expression in the adipose tissues of obese mice. Proc Natl Acad Sci USA. 1998;95:7591–6. [PubMed: 9636194]
18. Samad F, and Ruf W. Inflammation, obesity, and thrombosis. Blood. 2013;122(20):3415–22. [PubMed: 24092932]
19. Wang J, Ciaraldi TP, and Samad F. Tissue factor expression in obese type 2 diabetic subjects and its regulation by antidiabetic agents. J Obes. 2015;2015:291209. [PubMed: 25861467]
20. Ruf W, and Samad F. Tissue factor pathways linking obesity and inflammation. Hamostaseologie. 2015;35(3):279–83. [PubMed: 25623940]
21. Kopec AK, Abrahams SR, Thornton S, Palumbo JS, Mullins ES, Divanovic S, et al. Thrombin promotes diet-induced obesity through fibrin-driven inflammation. J Clin Invest. 2017;127(8):3152–66. [PubMed: 28737512]

22. Morange PE, Bastelica D, Bonzi MF, Van Hoef B, Collen D, Juhan-Vague I, et al. Influence of t-pA and u-PA on adipose tissue development in a murine model of diet-induced obesity. Thromb Haemost. 2002;87(2):306–10. [PubMed: 11858492]

23. Hoover-Plow J, Ellis J, and Yuen L. In vivo plasminogen deficiency reduces fat accumulation. Thromb Haemost. 2002;87(6):1011–9. [PubMed: 12083480]

24. Selvarajan S, Lund LR, Takeuchi T, Craik CS, and Werb Z. A plasma kallikrein-dependent plasminogen cascade required for adipocyte differentiaion. Nature Cell Biol. 2001;3:267–75. [PubMed: 11231576]

25. Andronicos NM, Chen EI, Baik N, Bai H, Parmer CM, Kiosses WB, et al. Proteomics-based discovery of a novel, structurally unique, and developmentally regulated plasminogen receptor, Plg-RKT, a major regulator of cell surface plasminogen activation. Blood. 2010;115(7):1319–30. [PubMed: 19897580]

26. Comuzzie AG, Cole SA, Laston SL, Voruganti VS, Haack K, Gibbs RA, et al. Novel genetic loci identified for the pathophysiology of childhood obesity in the Hispanic population. PLoS One. 2012;7(12):e51954. [PubMed: 23251661]

27. Lighvani S, Baik N, Diggs JE, Khaldoyanidi S, Parmer RJ, and Miles LA. Regulation of macrophage migration by a novel plasminogen receptor Plg-R KT. Blood. 2011;118(20):5622–30. [PubMed: 21940822]

28. Miles LA, Baik N, Lighvani S, Khaldoyanidi S, Varki NM, Bai H, et al. Deficiency of plasminogen receptor, Plg-RKT, causes defects in plasminogen binding and inflammatory macrophage recruitment in vivo. J Thromb Haemost. 2017;15(1):155–62. [PubMed: 27714956]

29. Thaler B, Baik N, Hohensinner PJ, Baumgartner J, Panzenbock A, Stojkovic S, et al. Differential expression of Plg-RKT and its effects on migration of proinflammatory monocyte and macrophage subsets. Blood. 2019;134(6):561–7. [PubMed: 31221672]

30. Vago JP, Sugimoto MA, Lima KM, Negreiros-Lima GL, Baik N, Teixeira MM, et al. Plasminogen and the Plasminogen Receptor, Plg-RKT, Regulate Macrophage Phenotypic, and Functional Changes. Front Immunol. 2019;10:1458. [PubMed: 31316511]

31. Miles LA, Baik N, Bai H, Makarenkova HP, Kiosses WB, Krajewski S, et al. The plasminogen receptor, Plg-RKT, is essential for mammary lobuloalveolar development and lactation. J Thromb Haemost. 2018;16(5):919–32. [PubMed: 29495105]

32. Wang J, Badeanlou L, Bielawski JD, Ciaraldi TP, and Samad F. Sphingosine Kinase 1 Regulates Adipose Proinflammatory Responses and Insulin Resistance. Am J Physiol Endocrinol Metab. 2014.

33. Mota de Sa P, Richard AJ, Hang H, and Stephens JM. Transcriptional Regulation of Adipogenesis. Compr Physiol. 2017;7(2):635–74. [PubMed: 28333384]

34. Bai H, Baik N, Kiosses WB, Krajewski S, Miles LA, and Parmer RJ. The novel plasminogen receptor, plasminogen receptor(KT) (Plg-R(KT)), regulates catecholamine release. J Biol Chem. 2011;286(38):33125–33. [PubMed: 21795689]

35. Betz MJ, and Enerback S. Targeting thermogenesis in brown fat and muscle to treat obesity and metabolic disease. Nat Rev Endocrinol. 2018;14(2):77–87. [PubMed: 29052591]

36. Gao P, Jiang Y, Wu H, Sun F, Li Y, He H, et al. Inhibition of Mitochondrial Calcium Overload by SIRT3 Prevents Obesity- or Age-Related Whitening of Brown Adipose Tissue. Diabetes. 2020;69(2):165–80. [PubMed: 31712319]

37. Kotzbeck P, Giordano A, Mondini E, Murano I, Severi I, Venema W, et al. Brown adipose tissue whitening leads to brown adipocyte death and adipose tissue inflammation. J Lipid Res. 2018;59(5):784–94. [PubMed: 29599420]

38. Grove LM, Southern BD, Jin TH, White KE, Paruchuri S, Harel E, et al. Urokinase-type plasminogen activator receptor (uPAR) ligation induces a raft-localized integrin signaling switch that mediates the hypermotile phenotype of fibrotic fibroblasts. J Biol Chem. 2014;289(18):12791–804. [PubMed: 24644284]

39. Feng B, Jiao P, Nie Y, Kim T, Jun D, van Rooijen N, et al. Clodronate liposomes improve metabolic profile and reduce visceral adipose macrophage content in diet-induced obese mice. PLoS One. 2011;6(9):e24358. [PubMed: 21931688]

40. Nawaz A, Aminuddin A, Kado T, Takikawa A, Yamamoto S, Tsuneyama K, et al. CD206(+) M2-like macrophages regulate systemic glucose metabolism by inhibiting proliferation of adipocyte progenitors. Nat Commun. 2017;8(1):286. [PubMed: 28819169]
41. Kanda H, Tateya S, Tamori Y, Kotani K, Hiasa K, Kitazawa R, et al. MCP-1 contributes to macrophage infiltration into adipose tissue, insulin resistance, and hepatic steatosis in obesity. J Clin Invest. 2006;116(6):1494–505. [PubMed: 16691291]
42. Kamei N, Tobe K, Suzuki R, Ohsugi M, Watanabe T, Kubota N, et al. Overexpression of monocyte chemoattractant protein-1 in adipose tissues causes macrophage recruitment and insulin resistance. J Biol Chem. 2006;281(36):26602–14. [PubMed: 16809344]
43. Spencer M, Yao-Borengasser A, Unal R, Rasouli N, Gurley CM, Zhu B, et al. Adipose tissue macrophages in insulin-resistant subjects are associated with collagen VI and fibrosis and demonstrate alternative activation. Am J Physiol Endocrinol Metab. 2010;299(6):E1016–27. [PubMed: 20841504]
44. Lighvani S, Baik N, Diggs JE, Khaldoyanidi S, Parmer RJ, and Miles LA. Regulation of macrophage migration by a novel plasminogen receptor Plg-R KT. Blood. 2011;118(20):5622–30. [PubMed: 21940822]
45. Bugge TH, Flick MJ, Daugherty CC, and Degen JL. Plasminogen deficiency causes severe thrombosis but is compatible with development and reproduction. Genes Dev. 1995;9:794–807. [PubMed: 7705657]
46. Ploplis VA, French EL, Carmeliet P, Collen D, and Plow EF. Plasminogen deficiency differentially affects recruitment of inflammatory cell populations in mice. Blood. 1998;91(6):2005–9. [PubMed: 9490683]
47. Nishimura S, Manabe I, Nagasaki M, Eto K, Yamashita H, Ohsugi M, et al. CD8+ effector T cells contribute to macrophage recruitment and adipose tissue inflammation in obesity. Nat Med. 2009;15(8):914–20. [PubMed: 19633658]
48. Divoux A, Tordjman J, Lacasa D, Veyrie N, Hugol D, Aissat A, et al. Fibrosis in human adipose tissue: composition, distribution, and link with lipid metabolism and fat mass loss. Diabetes. 2010;59(11):2817–25. [PubMed: 20713683]
49. Marcelin G, and Clement K. [Adipose tissue fibrosis: an aggravating factor in obesity]. Med Sci (Paris). 2018;34(5):424–31. [PubMed: 29900845]
50. Day F, Karaderi T, Jones MR, Meun C, He C, Drong A et al. Large-scale genome-wide meta-analysis of polycystic ovary syndrome suggests shared genetic architecture for different diagnosis criteria. PLOS Genetics.2018;14(12):e1007813. [PubMed: 30566500]
51. Liu M, Hummitzsch K, Hartanti MD, Rosario R, Bastian NA, Hatzirodos N, et al. Analysis of expression of candidate genes for polycyctic ovary syndrome in adult and fetal human and boine ovaries. Biology of Reproduciton. 2020;103(4):840–853.

Essentials

- Plg-R_{KT}, a unique transmembrane plasminogen receptor, enhances the activation of plasminogen to plasmin, and localizes the proteolytic activity of plasmin on the cell surface
- Mice genetically deficient in Plg-R_{KT} and littermate controls fed a high fat diet or control low fat diet were used to determine the role of Plg-R_{KT} in insulin resistance, glucose tolerance, T2D, and associated mechanisms including adipose inflammation, fibrosis and ectopic lipid storage
- Plg-R_{KT} deficient mice, when fed a high fat diet, gained more weight, developed more hepatic steatosis and were more insulin resistant/glucose intolerant than high fat diet-fed wild type littermates; and mechanistically, these metabolic defects were linked with increased AT inflammation, AT macrophage and T cell accumulation, adipose and hepatic fibrosis, and decreased insulin signaling in the AT and liver
- Plg-R_{KT} regulated the expression of PPARγ and other adipogenic molecules, suggesting a novel role for Plg-R_{KT} in the adipogenic program

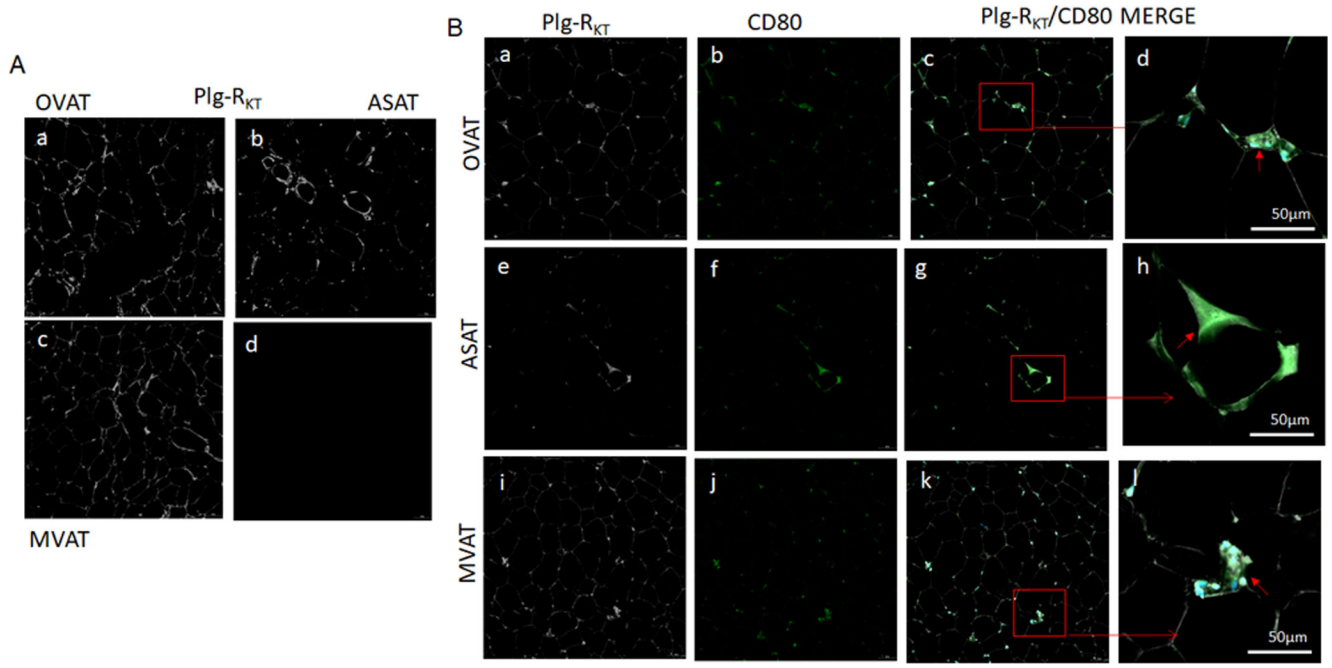

Figure 1. Plg-R_{KT} is expressed in human adipose tissues (AT).

Panel A: Plg-R_{KT} in adipocytes from human adipose tissue (AT) depots of bariatric surgery patients. Abdominal subcutaneous adipose tissue (ASAT) was taken superficial to the abdominal fascia/muscles, omental visceral adipose tissues (OVAT) was from the fat of the greater omentum, and mesenteric visceral adipose tissue (MVAT) was from the fat of the mesentery. Immunofluorescence staining of Plg-R_{KT} (white) is seen around the rim of adipocytes from (A-a) OVAT, (A-b) ASAT, and (A-c) MVAT. (A-d) Negative staining of OVAT without the primary anti-Plg-R_{KT} antibody. Panel B: Plg-R_{KT} in macrophages from human AT depots of bariatric surgery patients. Immunofluorescence staining of Plg-R_{KT} (white) in AT from OVAT (B-a), ASAT (B-e) and MVAT (B-i), respectively. Immunofluorescence staining of macrophages with CD80 (green) from OVAT (B-b), ASAT (B-f) and MVAT (B-j) respectively. Merged images of Plg-R_{KT} and CD80 staining in the respective AT depots indicating Plg-R_{KT} staining in AT macrophages. (B-c,d) Merged images of panels (B-a) and (B-b) indicating Plg-R_{KT} expression in OVAT macrophages. (B-g,h) Merge of panels (B-e) and (B-f) indicating Plg-R_{KT} expression in ASAT macrophages, (B-k,j) Merged images of panels B-i and B-j indicating Plg-R_{KT} expression in MVAT macrophages. Arrows indicate crown like structures. All images were acquired on a Zeiss "Observer Z1" inverted microscope, using an automated slide scanning stage (TissueFAXS, TissueGnostics, Austria) and a Hamamatsu fluorescence camera. For panels A-a through A-d and for all panels in Fig. 1B except for B-d, B-h and B-I Magnification = 200X. For higher magnification panels B-d,B-h and B-j scale bar = 50μm

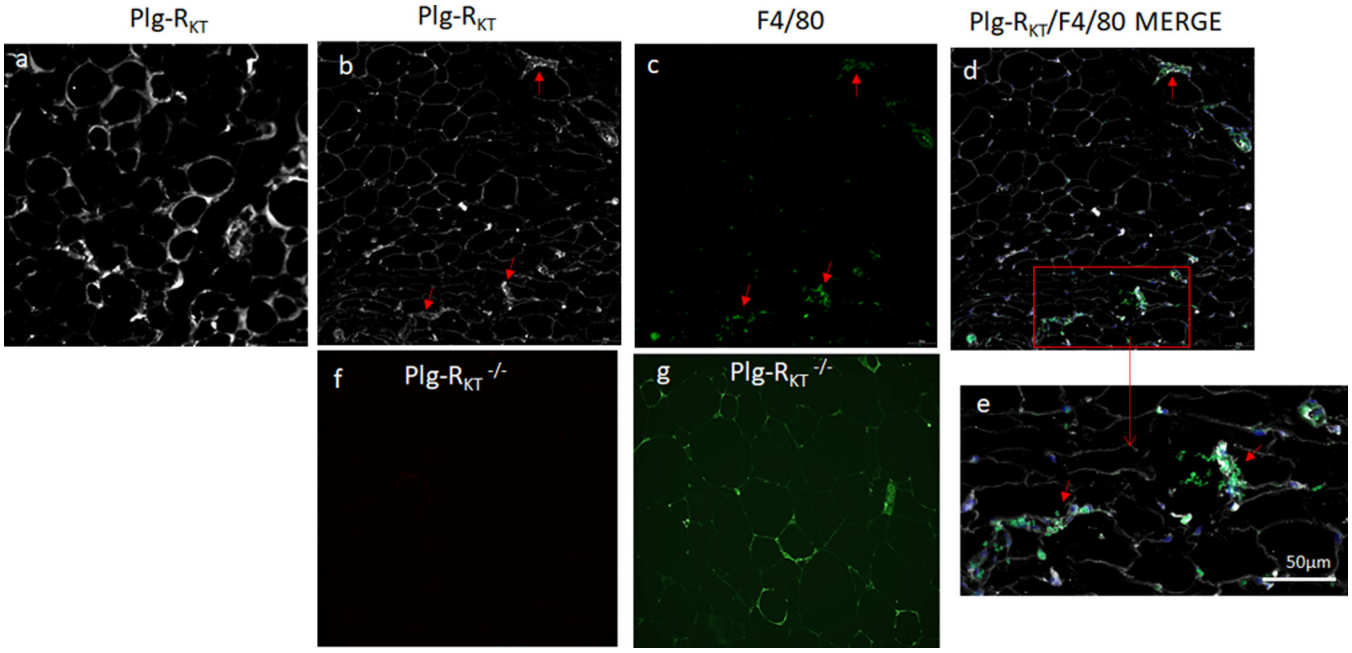

Figure 2: Plg-R$_{KT}$ is expressed in mouse adipose tissues (AT). Plg-R$_{KT}$ expression in EAT of HFD-fed obese C57BL/6J mice.

Representative immunofluorescence staining showing staining of Plg-R$_{KT}$ (white) around adipocytes of male C57BL/6J mice fed a HFD for 16 weeks (Panel a). Immunofluorescence staining of macrophages with Plg-R$_{KT}$ (white: panel b) and F4/80 (green: Panel c) in epididymal AT of HFD-fed male C57BL/6J mice. Merged images of panels b and c showing Plg-R$_{KT}$ expression in AT macrophages. (Panels d, e). Arrows indicate crown like structures. Negative control for Plg-R$_{KT}$ staining in Plg-R$_{KT}$ deficient mice (panel f). F4/80 staining in Plg-R$_{KT}$ deficient mice (panel g). All images were acquired on a Zeiss “Observer Z1” inverted microscope, using an automated slide scanning stage (TissueFAXS, TissueGnostics, Austria) and a Hamamatsu fluorescence camera. For panels a-d and f-g, Magnification = 200X. For higher magnification panel e, scale bar = 50µm.

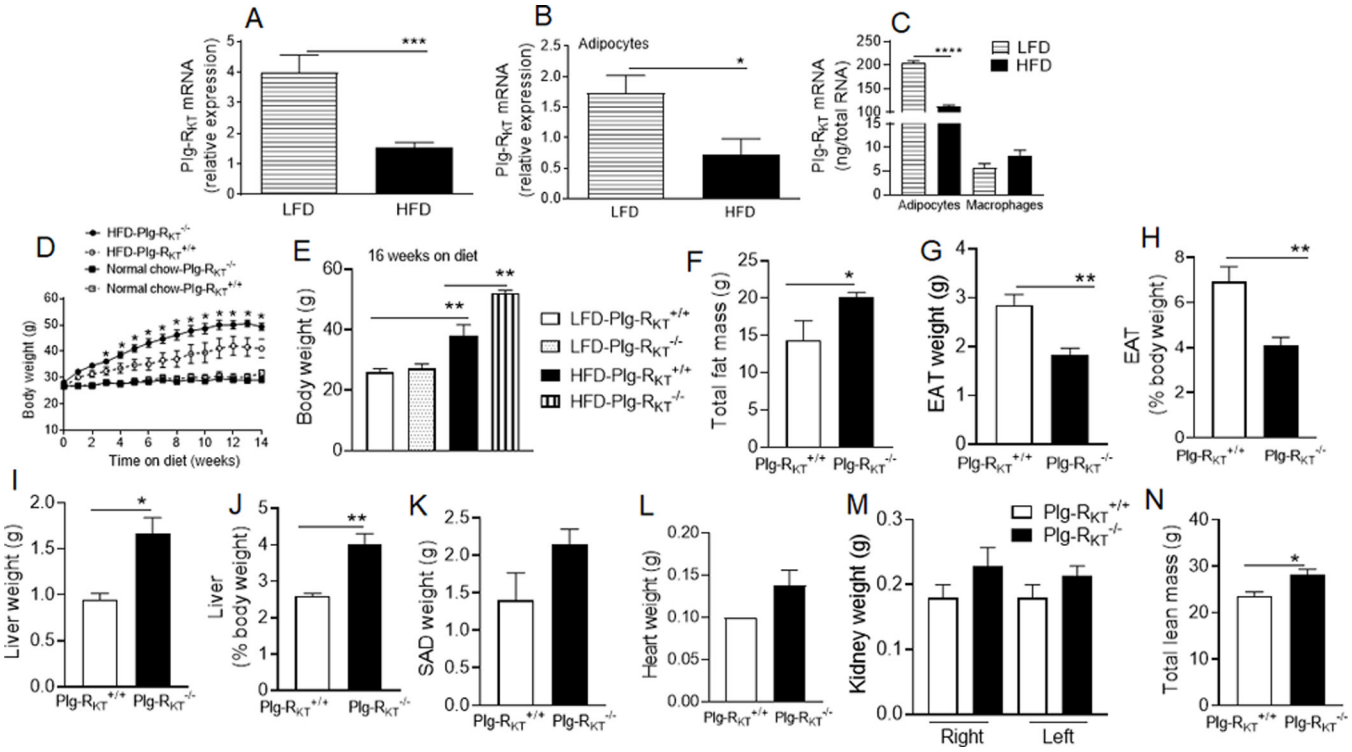

Figure 3. Plg-R_{KT} regulates weight gain and fat mass distribution:

(A) Plg-R_{KT} mRNA expressed in male C57BL/6J mice in epididymal AT on either a low fat (normal chow) diet (LFD, 10% fat) or a high fat diet (HFD, 60% fat) for 16 weeks. (B) Plg-R_{KT} mRNA in isolated adipocytes from epididymal AT of LFD and HFD fed mice. For (A) and (B) n = 6 ± SEM. *P < 0.05, ***P < 0.001, LFD versus HFD. (C) Plg-R_{KT} mRNA measured by ddPCR in adipocytes and in AT macrophages from epididymal AT of LFD and HFD fed mice. For (C) n = 4 ± SEM. ****P < 0.0001, LFD versus HFD. (D) Body weights of Plg-$R_{KT}^{-/-}$ and Plg-$R_{KT}^{+/+}$mice on either a LFD or HFD determined over 14 weeks, n = 12 ± SEM. (E) Body weights of Plg-$R_{KT}^{-/-}$ and Plg-$R_{KT}^{+/+}$mice on either a LFD or HFD determined at 16 weeks, n = 6 ± SEM. For (D) and (E) *P < 0.05, *P < 0.05, **P < 0.01 for HFD-fed Plg-$R_{KT}^{-/-}$ vs Plg-$R_{KT}^{+/+}$mice. (F)(G)(H) Total fat mass and epididymal AT weights respectively of 16 weeks HFD-fed Plg-$R_{KT}^{-/-}$ and Plg-$R_{KT}^{+/+}$ mice. n = 6–8 ± SEM. (I)(J) Liver weights of 16 weeks HFD-fed Plg-$R_{KT}^{-/-}$ and Plg-$R_{KT}^{+/+}$mice. For (F)-(J) n = 6 ± SEM, *P < 0.05, **P < 0.01 for HFD-fed Plg-$R_{KT}^{-/-}$ vs Plg-$R_{KT}^{+/+}$mice. (K)(L)(M)(N) SAD, Heart, kidney, and total lean mass respectively of 16 week HFD-fed Plg-$R_{KT}^{-/-}$ and Plg-$R_{KT}^{+/+}$ mice. n = 6–8 ± SEM; For (N) *P < 0.05, for HFD-fed Plg-$R_{KT}^{-/-}$ vs Plg-$R_{KT}^{+/+}$mice.

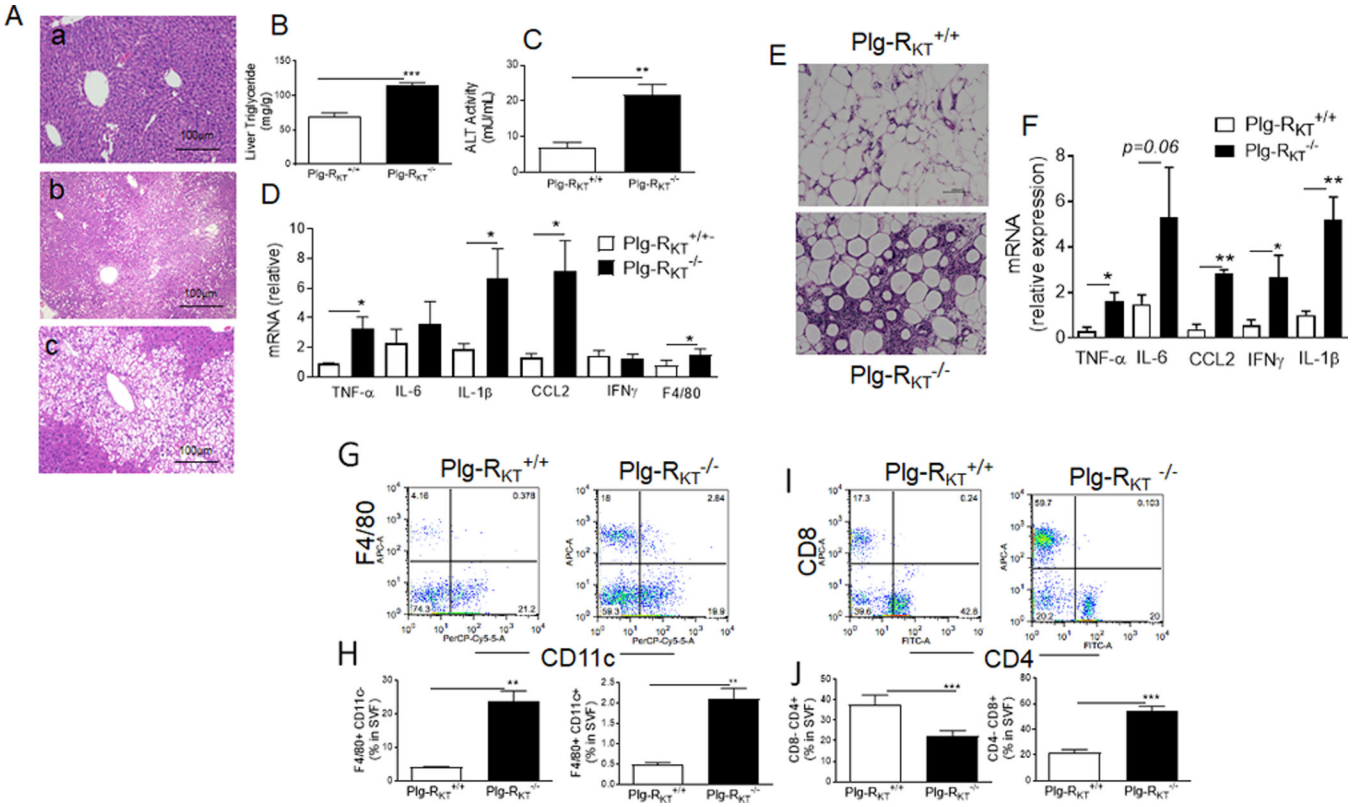

Figure 4. Deletion of Plg-R_{KT} promotes hepatic steatosis and adipose inflammation.

(A) Representative H&E-stained paraffin-embedded sections of liver from 16-week normal chow LFD -fed Plg-$R_{KT}^{+/+}$ wild type mice (A-a), HFD-fed Plg-$R_{KT}^{+/+}$ mice (A-b) and HFD-fed Plg-$R_{KT}^{-/-}$ (A-c). (B) Liver triglyceride and (C) Plasma ALT activity of HFD-fed Plg-$R_{KT}^{-/-}$ and Plg-$R_{KT}^{+/+}$ mice. For (B) and (C) n = 4–7 ± SEM. **P < 0.01, ***P < 0.001 for Plg-$R_{KT}^{-/-}$ vs Plg-$R_{KT}^{+/+}$mice. (D) Cytokine/chemokine expression in livers of HFD-fed Plg-$R_{KT}^{-/-}$ and Plg-$R_{KT}^{+/+}$ mice. For (D), n=8 ± SEM, *P < 0.05 for HFD-fed Plg-$R_{KT}^{-/-}$ vs Plg-$R_{KT}^{+/+}$mice. (E) Representative H & E sections and (F) Cytokine/chemokine expression of epididymal AT from 16-week HFD-fed Plg-$R_{KT}^{-/-}$ and Plg-$R_{KT}^{+/+}$ mice. For panel (F) n = 5 ± SEM. *P < 0.05, **P < 0 01 for Plg-$R_{KT}^{-/-}$ vs Plg-$R_{KT}^{+/+}$mice. (G)(H) FACS quantification of F4/80+/CD11c- and F4/80+/CD11c+ macrophage populations in SVF cells of epididymal AT of HFD-fed Plg-$R_{KT}^{-/-}$ and Plg-$R_{KT}^{+/+}$. Cells from 2–3 mice were pooled. n = 3 ± SEM. **P < 0.01 for Plg-$R_{KT}^{-/-}$ vs Plg-$R_{KT}^{+/+}$mice. (I)(J) FACS quantification of CD4+ and CD8+ T-cell populations in SVF cells of epididymal AT of HFD-fed Plg-$R_{KT}^{-/-}$ and Plg-$R_{KT}^{+/+}$. Cells from 2–3 mice were pooled. n = 3 ± SEM. ***P < 0.001 for Plg-$R_{KT}^{-/-}$ vs Plg-$R_{KT}^{+/+}$mice. Scale bar for (A) and (E) = 100μm.

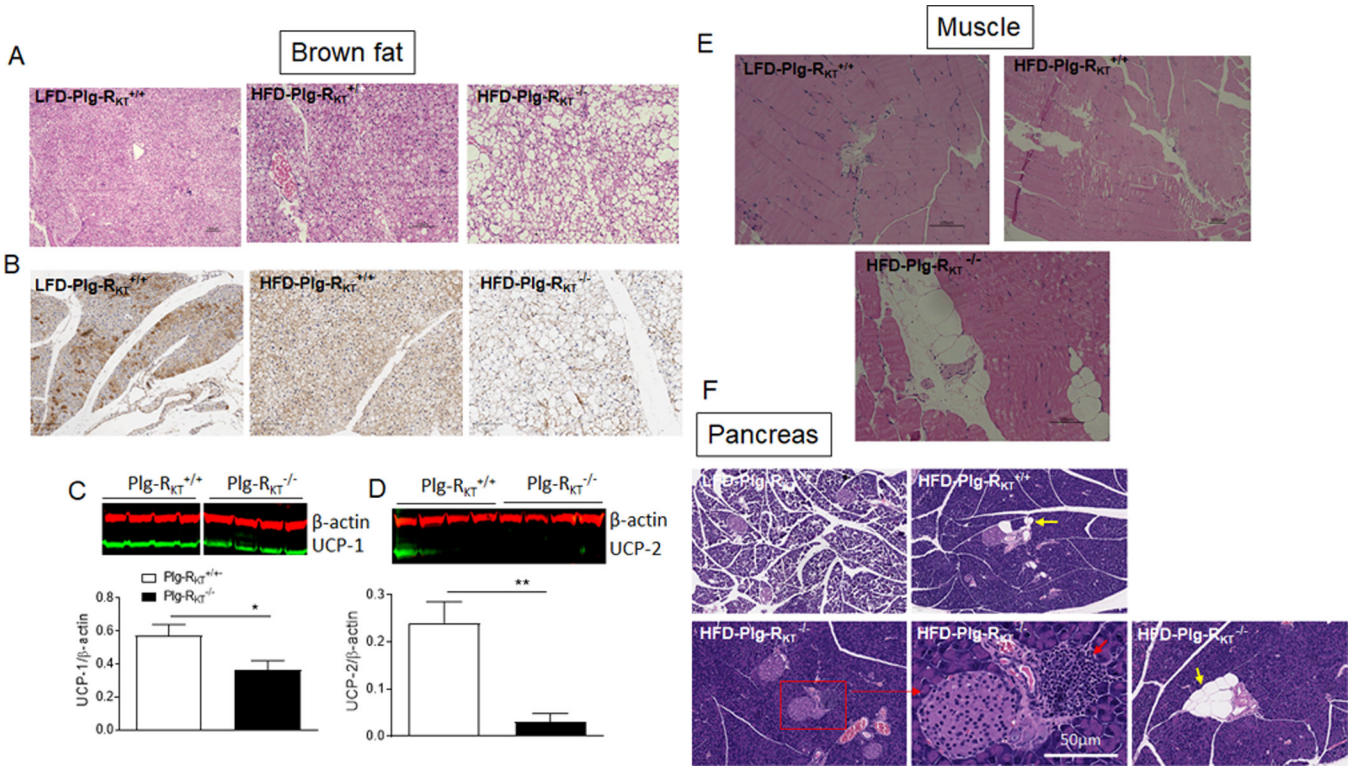

Figure 5. Deletion of Plg-R$_{KT}$ promotes lipid deposition in other insulin-sensitive tissues.

Representative H & E staining of sections of brown fat (A), Immunohistology for UCP-1 in brown fat (B) and western blot analysis for UCP-1 and UCP-2 (C, D) expression in brown fat of 16-week HFD-fed Plg-R$_{KT}^{-/-}$ vs Plg-R$_{KT}^{+/+}$mice. For (C) and (D), n=4 ± SEM. *P < 0.05, **P < 0 01 for Plg-R$_{KT}^{-/-}$ vs Plg-R$_{KT}^{+/+}$mice. (E) Representative H & E sections of skeletal muscle of 16-week LFD fed wildtype Plg-R$_{KT}^{+/+}$, HFD-fed Plg-R$_{KT}^{+/+}$ and Plg-R$_{KT}^{-/-}$ mice. (F) Representative H & E sections of pancreas of 16-week LFD fed wildtype Plg-R$_{KT}^{+/+}$ mice, HFD-fed Plg-R$_{KT}^{+/+}$ and Plg-R$_{KT}^{-/-}$ mice. Red arrow points to inflammatory cells. Yellow arrow points to lipid accumulation. Magnification for all images except for pancreas of HFD- Plg-R$_{KT}^{-/-}$ is x200. Scale bar for higher magnification HFD-Plg-R$_{KT}^{-/-}$ pancreas = 50μm.

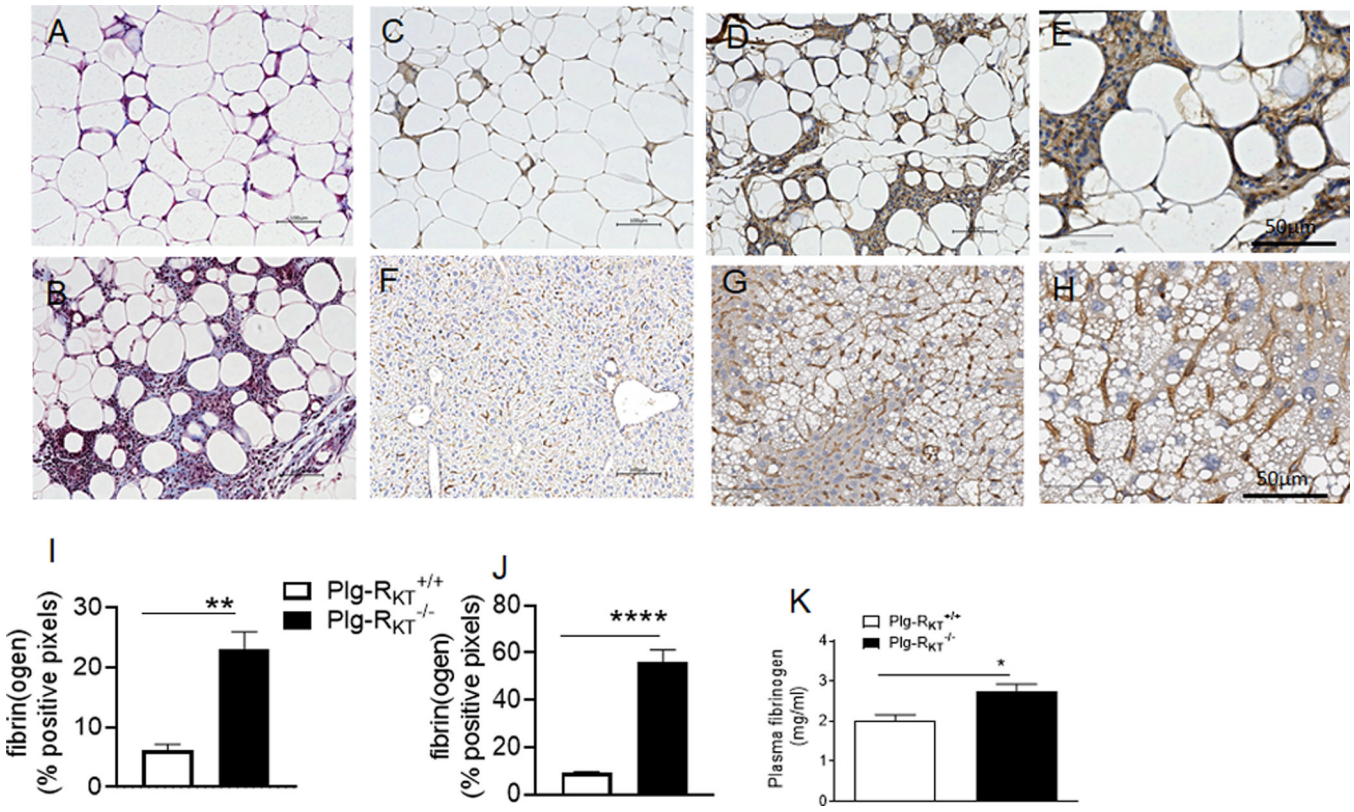

Figure 6. Deletion of Plg-R_{KT} promotes collagen and fibrin deposition.

Trichrome and fibrin staining was performed on sections of epididymal AT and liver collected after 16 weeks of HFD feeding. (A) (B) Trichrome staining of epididymal AT of Plg-$R_{KT}^{+/+}$ and Plg-$R_{KT}^{-/-}$ mice. (C) Fibrin immunostaining of epididymal AT of Plg-$R_{KT}^{+/+}$ mice. (D)(E) Low and high magnification respectively of fibrin immunostaining of epididymal AT of Plg-$R_{KT}^{-/-}$ mice. (F) Fibrin immunostaining of liver of Plg-$R_{KT}^{+/+}$ mice. (G)(H) Low and high magnification respectively of fibrin immunostaining of liver of Plg-$R_{KT}^{-/-}$ mice. Representative sections are shown. Magnification for all images except panels E and H is x200. Scale bar for higher magnification panels E and H= 50µm. (I)(J) Quantification of fibrin deposits in the epididymal AT and liver of Plg-$R_{KT}^{+/+}$ and Plg-$R_{KT}^{-/-}$ mice. Quantification of fibrin deposits was performed by using QuPath software. 4–6 fields per tissue were randomly selected for analysis using the pixel classification tool. n=4–6 ± SEM. **P < 0.01, ****P < 0 0001 for Plg-$R_{KT}^{-/-}$ vs Plg-$R_{KT}^{+/+}$mice. (K) Plasma fibrinogen levels in HFD-fed Plg-$R_{KT}^{+/+}$ and Plg-$R_{KT}^{-/-}$ mice, n=4–6 ± SEM. *P < 0.05 for Plg-$R_{KT}^{+/+}$ vs Plg-$R_{KT}^{-/-}$ mice.

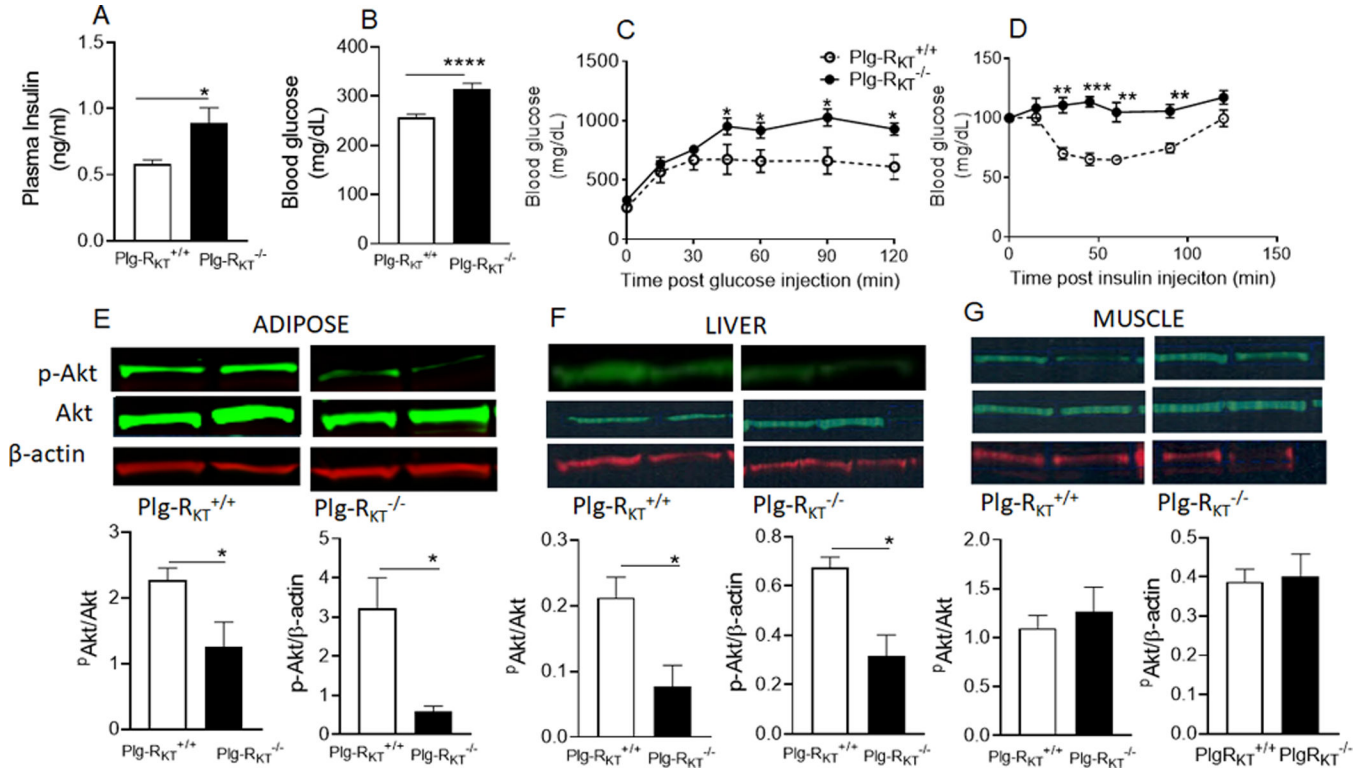

Figure 7. Plg-R_{KT} regulates glucose homeostasis and insulin resistance.

(A) Plasma insulin concentration, (B) Blood glucose concentration, (C) Glucose tolerance test, (D) Insulin tolerance test of HFD-fed Plg-$R_{KT}^{-/-}$ and Plg-$R_{KT}^{+/+}$ mice. (E)(F)(G) Representative western blots (of 2 representative mice) and densitometric scans of insulin-mediate Akt phosphorylation in epididymal AT, liver and muscle of HFD-fed Plg-$R_{KT}^{-/-}$ and Plg-$R_{KT}^{+/+}$ mice. For all panels, n = 4–6 ± SEM. *P < 0.05, **P < 0.01, ***P < 0.001 for Plg-$R_{KT}^{-/-}$ vs Plg-$R_{KT}^{+/+}$mice.

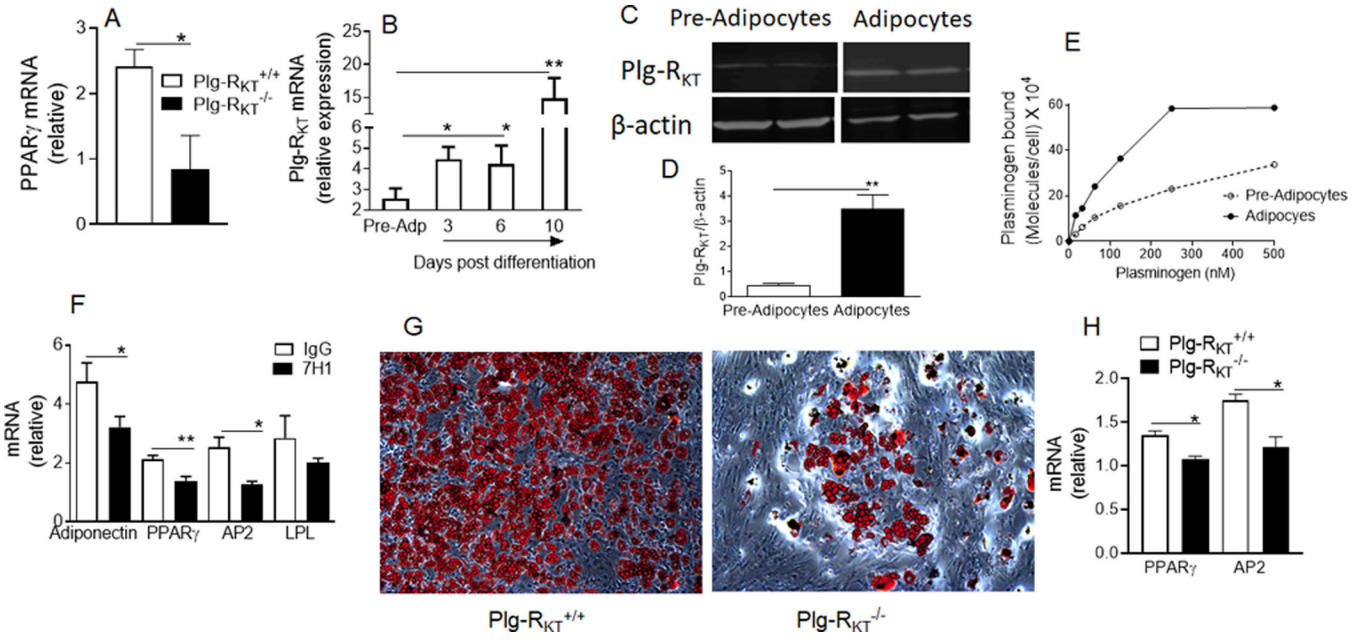

Figure 8. Plg-R_{KT} regulates adipogenesis.

(A) PPAR**γ** mRNA in HFD-fed epididymal AT of Plg-$R_{KT}^{-/-}$ and Plg-$R_{KT}^{+/+}$ mice. n = 6 ± SEM. *P < 0.05 for Plg-$R_{KT}^{-/-}$ vs Plg-$R_{KT}^{+/+}$mice. (B) Plg-R_{KT} mRNA during the course of adipogenesis of 3T3-L1 pre-adipocytes. n =6 ± SEM. *P < 0.05, **P < 0.01 for pre-adipocytes versus days post differentiation. (C) Western blots of Plg-R_{KT} protein expression in 3T3-L1 pre-adipocytes and adipocytes harvested at 10 days post-differentiation and (D) Densitometric quantification of Western blots, n =4 ± SEM. **P < 0.01 for pre-adipocytes versus adipocytes. (E) Plasminogen binding to 3T3-L1 preadipocytes versus adipocytes. Plasminogen binding to preadipocytes and adipocytes was measured by quantitative FACS equilibrium analysis with fluorescein isothiocyanate-labeled plasminogen as described(25). Specific binding was determined in the presence of epsilon aminocaproic acid, which inhibits the interaction of plasminogen with cells. Kd for Pre-adipocytes: 276±37 nM; Kd for adipocytes: 125±29 nM; Bmax for pre-adipocytes: 513,077±34,889, Bmax for adipocytes: 777,847±71,413. (F) Adipogenic gene expression during 3T3-L1 adipogenesis in the presence of anti- Plg-R_{KT} mAB (7H1) or IgG. n = 5 ± SEM. *P < 0.05, **P < 0.01 for mAb 7H1 versus control IgG. (G) Oil Red O staining and(H) adipogenic gene expression of primary adipocyte cultures derived from SVF cells from subcutaneous AT of Plg-$R_{KT}^{-/-}$ and Plg-$R_{KT}^{+/+}$ mice 10 days after differentiation. n = 3 ± SEM. *P < 0.05.